3D Reconstruction of Extended Target Signature with Distributed MIMO Radar Nodes

Kuitong Lou, Mareike Wendelmuth, Nicolas Kruse, Alexander Yarovoy, Francesco Fioranelli
Microwave Sensing, Signals & Systems (MS3) Group
Delft University of Technology
Delft, the Netherlands
(k.lou, m.wendelmuth, n.c.kruse, a.yarovoy, f.fioranelli)@tudelft.nl

2025 IEEE Radar Conference (RadarConf25) | 979-8-3315-4433-1/25/$31.00 ©2025 IEEE | DOI: 10.1109/RADARCONF2559087.2025.11204891

***Abstract*—The problem of reconstructing 3D signatures of human activities for monitoring and classification is considered in this work. A method based on data fusion from distributed MIMO (multiple-input multiple-output) radar nodes is developed in order to generate 3D intensity maps and related voxel-wise velocity vectors. The proposed method was evaluated with a dataset collected using three 60 GHz radars and including 7 activities performed by 30 participants. The results show that both static postures and dynamic activities can be captured effectively: consecutive phases of activities/movements can be identified by combining spatial intensity and velocity vectors, and the participant can be localized in the area under test. Furthermore, initial promising classification results of 98.3% macro F1-score are demonstrated in a three-class problem using the proposed 3D intensity maps and velocity vectors as inputs to a Convolutional Neural Network classifier.**

***Index Terms*—human activity recognition, distributed radar, MIMO, radar network.**

I. Introduction

The application of radar systems in healthcare has gained increasing attention over the last few years. In an aging society, health monitoring is a growing priority, especially when it can be performed in a contactless manner, with more comfort for patients/users and more safety for healthcare personnel [1]. This need was also dramatically highlighted by the COVID-19 pandemic. Radar systems are well-suited for contactless human monitoring due to their ability to operate in diverse environments without requiring wearable devices or specific light or environmental conditions, and also thanks to their privacy-preserving characteristics compared to video-based monitoring [2]. Embedding radars in a home or care environment (e.g., hospital, care home, psychiatric clinic) is therefore a promising technology for future healthcare applications [3].

Recent works in human activity recognition (HAR) have explored the use of 3D point cloud data generated by millimeter-wave (mmWave) multiple-input multiple-output (MIMO) radar systems. Specifically, these radar systems [4] [5] with a high number of virtual channels (e.g., 12 transmitters, 16 receivers) can allow richer and denser point cloud data, leading to improved classification performance. In parallel, other studies have investigated using more conventional radar signals and representations, e.g., micro-Doppler signatures used as images for classification without generating point clouds [6] [7]. However, these studies using a single radar sensor have limitations in fully capturing 3D kinematic information of the people's movement.

To overcome these limitations, distributed radar systems have emerged as a promising solution to the spatial limitations of single radars [8]. By utilizing multiple radar nodes, distributed systems can provide multi-view sensing compared to stand-alone radar. This can offer enhanced performance in classification, tracking, and vital sign estimation. For example, a MIMO radar network is introduced in [9] with two radars operating at 77 GHz and placed orthogonally for human activity recognition and fall detection. Radar data cubes composed of range, angle, and Doppler are used as input to a long-short-term-memory (LSTM) neural network for classification. Similarly, a distributed radar system consisting of two single-input single-output (SISO) radars is proposed in [10] to realize a direction-independent HAR. This system can allow capturing multidirectional human movements from two perspectives. Two distinct micro-Doppler signatures are computed and then fused by a deep convolutional neural network (DCNN) to identify five activities regardless of their direction of motion.

While distributed radar systems have been demonstrated in the literature, these are typically deployed at chest/hip height and relatively close to the patients/users. This is not possible in certain contexts, such as in psychiatric clinics, where the radars must be out of the reach of patients, and in general, a deployment that is as unobtrusive as possible for the 'normal', familiar environment of the users is preferable. In this regard, deployment on an elevated position, such as the ceiling, can be beneficial for monitoring, although it is relatively under-explored in the literature with few exceptions [11], [12]. Moreover, challenges for effective monitoring include the capability to capture both static postures and complex kinematic movements. 2D representations, such as micro-Doppler or even point clouds from a single radar, may not be sufficient to distinguish between similar motions and localize activities accurately. Thus, reconstructing detailed 3D signatures is crucial to distinguish different motions and postures.

To start addressing the aforementioned challenges, this work proposes a distributed radar fusion method for HAR using 60 GHz MIMO radar nodes. The method reconstructs 3D intensity maps of the person in the monitored area and voxel-wise velocity vectors by fusing data cubes from multiple

radar nodes. Compared to the method in [13], which uses multilateration with five ultra-wideband (UWB) radar nodes aligned in a 2D semi-circular baseline, the proposed approach leverages MIMO beamforming to achieve improved 3D reconstruction of signatures. The fusion of range-azimuth-elevation data cubes preserves accurate mapping of the person shape in the resulting 3D grid by combining complementary views from multiple perspectives; this also enables the estimation of complete velocity vectors for different body parts. The feasibility of the proposed method to generate intensity maps & voxel-wise velocity vectors is demonstrated with experimental data collected with 30 participants performing 7 activities.

The rest of this paper is organized as follows. Section II describes the proposed methodology to reconstruct extended target signatures with distributed MIMO radars. Section III presents details of the experimental dataset collected, with initial feasibility results in Section IV. Finally, conclusions are drawn in Section V.

II. Proposed Methodology

In this paper, a methodology to achieve data fusion in a distributed network of MIMO radar is presented, with the ultimate objective to improve human activity classification. Specifically, the proposed approach utilizes range-azimuth-elevation information from each radar in the network to then reconstruct overall 3D intensity maps and velocity vectors. The processing steps are described in this section, with qualitative results in terms of 3D representations and quantitative results in terms of F1-score from classification presented in the later section IV.

A. Radar Signal Processing Pipeline

Fig. 1 illustrates the envisaged radar signal processing pipeline. For each MIMO radar node, a Fast Fourier Transform (FFT) is first applied to the raw data across the fast time domain to perform range estimation. Static clutter removal is performed in each frame to attenuate the contribution of static clutter. Subsequently, a FFT across the slow time domain is performed to calculate the range-Doppler map. Then, target detection is performed to identify the range bins occupied by the target to reduce the subsequent computational load. Capon beamforming is then applied on such range bin data to estimate the angular information of the target, specifically azimuth and elevation at the dominant Doppler values above a defined threshold. The threshold is set 20 dB above the estimated noise floor in the range-Doppler map. As a result, a 3D real-valued radar data cube of the spatial power spectrum is generated per frame, with dimensions range $\times$ azimuth $\times$ elevation.

It should be noted that for static targets such as a person in a stationary posture while standing or lying, the static clutter removal in the frame can also unavoidably remove part of the target signature. For this reason, only range information across multiple chirps of a detected target in a frame is used for angular estimation.

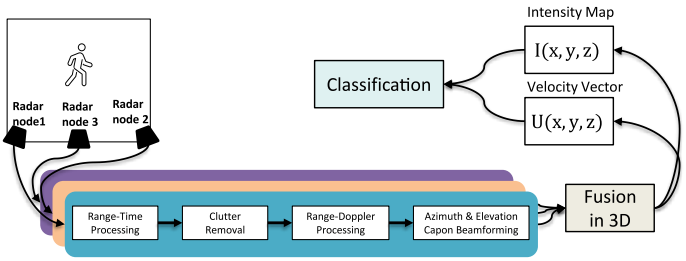

Fig. 1: Processing pipeline for the proposed radar fusion method using a distributed MIMO radar network.

B. Distributed Radar Fusion

The proposed distributed radar fusion method takes as input the 3D radar data cubes from each radar, computed as described in the previous sub-section, i.e., using FFT processing for Doppler estimation and Capon beamforming for angular estimation. In the first step of the fusion method, the 3D space of the target moving area is uniformly voxelized in Cartesian coordinates. The 3D space is discretized into a uniform voxel grid, with $i \in 1, \ldots, N_x$, $j \in 1, \ldots, N_y$, and $k \in 1, \ldots, N_z$ indexing the grid points along the x-, y-, and z-axes, respectively.

1) Intensity Map : For each frame, N 3D radar data cubes from N distributed radar nodes are generated, serving as input to the fusion method. With the radar data cubes and known positions of radars (x_n, y_n, z_n), the measured signal intensity I at an arbitrary voxel (x_i, y_j, z_k) can be determined by computing the range, elevation, and azimuth with respect to all N radars. The range r_n from the n-th radar to a voxel in the 3D space is computed as:

$$r_n = \sqrt{(x_i - x_n)^2 + (y_j - y_n)^2 + (z_k - z_n)^2}, \quad (1)$$

while the azimuth θ_n and elevation ϕ_n angles are calculated by:

$$\theta_n = \tan^{-1}\left(\frac{y_j - y_n}{x_i - x_n}\right), \quad (2)$$

$$\phi_n = \sin^{-1}\left(\frac{z_k - z_n}{r_n}\right). \quad (3)$$

Then, inspired by the work of [13], the intensity map is aggregated across all radar nodes based on their respective power spectra to reconstruct the 3D intensity map $I(x, y, z)$. For each voxel and radar node n at timestamp t, the aggregated intensity map is computed as:

$$I(x, y, z, t) = \sum_{n=1}^{N} P_n(r_n, \phi_n, \theta_n, t), \quad (4)$$

where P_n denotes the 3D radar data cube obtained from Capon beamforming for n-th radar node at timestamp t.

2) Velocity Vector: The velocity vector $\mathbf{U}(x, y, z) = [u_x, u_y, u_z]^T$ is reconstructed for each voxel by solving a system of linear equations derived from radial velocity projections measured by N radar nodes using least-squares optimization. Each radar measures a radial velocity $v_{r,n}$, which is the

projection of the voxel's velocity onto the unit vector $\hat{r}_n$ pointing from the voxel to the radar, as:

$$v_{r,n} = \mathbf{U} \cdot \hat{r}_n. \tag{5}$$

By collecting the measurements from all radar nodes, this can be written in matrix form as:

$$\mathbf{v}_r = \mathbf{R}\mathbf{U}, \quad \text{with} \quad \mathbf{v}_r = \begin{bmatrix} v_{r,1} \\ v_{r,2} \\ \vdots \\ v_{r,N} \end{bmatrix}, \quad \mathbf{R} = \begin{bmatrix} \hat{r}_1^T \\ \hat{r}_2^T \\ \vdots \\ \hat{r}_N^T \end{bmatrix}$$

Here, $\mathbf{R}$ is an $N \times 3$ matrix composed of unit direction vectors, and $\mathbf{v}_r$ is an $N \times 1$ vector of observed radial velocities.

The least-squares solution minimizes the squared error between the measured and modeled radial velocities as:

$$\min_{\mathbf{U}} \|\mathbf{R}\mathbf{U} - \mathbf{v}_r\|_2^2$$

Accordingly, the velocity vector $\mathbf{U}$ is estimated using the least-squares solution as derived in [13]:

$$\mathbf{U} = (\mathbf{R}^T\mathbf{R})^{-1}\mathbf{R}^T\mathbf{v}_r.$$

Both intensity maps and velocity vectors per voxel can later be used as input data to classification processes for human activity classification.

III. Dataset

In this section, the collected dataset to validate the proposed approach is briefly described.

A. Experimental Setup

The proposed distributed radar network consists of three 60 GHz IWR6843ISK MIMO radars by Texas Instruments (TI) [14], which are located as shown in Fig. 2. Two radar nodes, Radar #1 & Radar #2, are mounted on the ceiling at an elevated and tilted position to illuminate the area under test. The third radar, Radar #3, is placed on the wall with a height of approximately 1 m without any rotation and is used for further validation and comparison. It should be noted that this specific deployment of the radar nodes on the ceiling was dictated by the end-users' application requirements to have the sensors out of the way of the people or patients being monitored. This is of particular importance in, for example, the context of psychiatric clinics, as discussed in the companion paper on vital sign estimation in this configuration [15].

The three radars operated in Frequency Division Multiplexing Access (FDMA) mode at starting frequencies of 60, 61.25, and 62.5 GHz with a bandwidth of 1 GHz, resulting in a range resolution of 15 cm. This was done to avoid potential mutual interference due to overlapping bands. The detailed parameters of the radar waveforms are given in Table I.

Before the measurements with the participants, calibration for the two elevated and tilted radars is performed. A corner reflector was placed at different positions in the area under test depicted in Fig. 3. With this, the necessary compensations for the tilting of the radars in azimuth and elevation angles are calculated for the subsequent fusion.

The area under test where participants were asked to move was limited in range between points A, B, and C, as shown in Fig. 3 in the dark gray area. The wall where the radars were placed is assumed to be the Y-Z plane in the chosen coordinate system of this work. Therefore, the coordinates of the three radars are set as (0, 0, 270), (0, 500, 270), and (0, 250, 100) with the unit of cm, respectively.

TABLE I: Radar Waveform and Processing Parameters

Parameter	Value
Start frequency	60, 61.25, 62.5 GHz
Chirp Bandwidth	1 GHz
Sample Rate	2000 ksps
Chirps per Frame	120
Frame duration	100 ms
Active TX	3
Active RX	4
Azimuth resolution	14 deg
Elevation resolution	57 deg
Maximum range	11.99 m
Range resolution	0.15 m
Maximum velocity	3.1 m/s
Velocity resolution	0.15 m/s

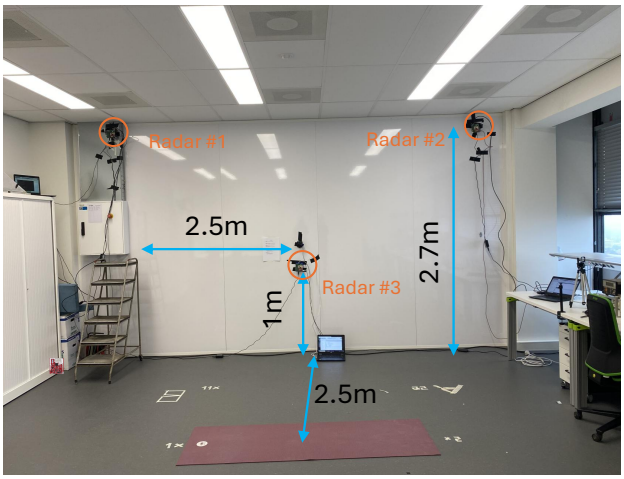

Fig. 2: Experimental setup with the three radars. Radar #1 and Radar #2 are mounted near the ceiling with tilted and rotated line of sight. Radar #3 is placed at hip height with straight field of view towards the area under test.

B. Human Activities

The choice of the recorded activities in this specific data collection was inspired by the insights of collaborators from the Psychiatry Department of the Erasmus Medical Center, Rotterdam, and other mental health institutions. These comprised a combination of static postures and movements, including examples of fast and unforeseen movements such as boxing in the air or jumping jacks, with the aim of reproducing sudden movements at times performed by psychiatric patients. Each participant was asked to perform 7 activities, with a recording duration of 1 minute per activity.

1) Walking: The participant walked along a triangular trajectory, starting at point A, then to B, to C and back to point A shown in Fig. 3.

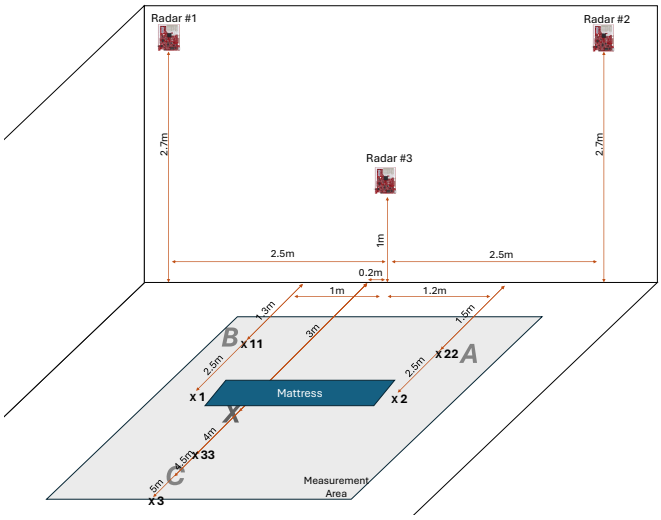

Fig. 3: Sketch of the experimental setup with the 3 radars and distances/sizes of the area under test.

2) Jumping Jacks: The participant was asked to perform Jumping Jacks continuously at point X in Fig. 3.
3) Boxing / Kicking: The participant should pretend to box and kick the air for this activity.
4) Turning / Restless: The participant was asked to turn around or show restless movement while lying on the floor on a mattress.
5) Sitting: The participant had to sit on the mattress facing the wall.
6) Lying on the back: The participant lies on their back on the mattress.
7) Lying on the side: The participant lies on their side on the mattress.

The recordings of the activity 'jumping jacks' and 'boxing/kicking in the air' were split into two sequences of 30 s, allowing two different positions and a short rest of 10 s in between. In total, 30 participants took part in the experiment, with 23 males and 7 females. The mean age of the participants was 30.7 years with a standard deviation (STD) of 7.6 years, and the average height was 178.3 cm with a STD of 6.7 cm. Approval from the TU Delft Ethics Committee HREC was granted for this data collection.

IV. Results

In this section, qualitative and quantitative results for the proposed method are presented.

A. Qualitative 3D Signature Visualization

To demonstrate the capabilities of the proposed method for human activity recognition, qualitative results for radar imaging using both 3D intensity maps and estimated velocity vectors are presented and discussed. The 3D intensity maps $I(x, y, z)$ are constructed using Capon beamforming and radar data cubes from three radars, as discussed in Section II. The aim is to capture the spatial and kinematic dynamics of human activities, whether they are static postures or movements.

Fig. 4 shows top-views (X-Y plane) and front-views (Y-Z plane) slices of the intensity map and reconstructed velocity vectors during a jumping jack sequence across two consecutive frames. In the top-view slice shown in Fig. 4a, the velocity vectors appear to be smaller and constrained around the torso of the person. Conversely, Fig. 4b shows the velocity vectors extending outward, which corresponds to the outward motion of the participant's arms and legs, which extend while performing a jumping jack movement. Fig. 4c and Fig. 4d illustrate the jumping phase of the 'jumping jack' movement from front-views, where the Z axis is essentially the vertical (elevation) dimension. It should be noted that the time instances considered in these sub-figures differ from those considered in sub-figures 4a and 4b. In these examples, the velocity vectors clearly indicate the upward and downward motion as the participant leaves the ground while jumping upward, and then returns to the floor, respectively. These figures demonstrate the feasibility of the proposed method to resolve the different phases of dynamic human movements, both in terms of spatial occupancy of the body as well as directionality and magnitude of the velocity of the movements.

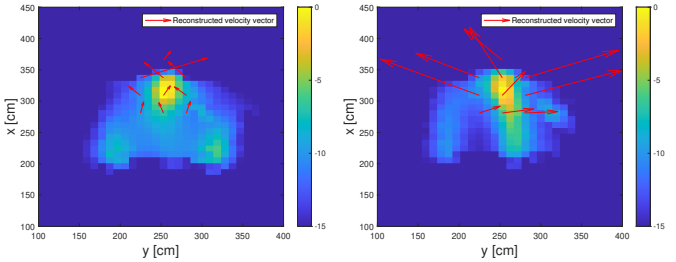

(a) Top-view showing torso-focused velocity vectors during a jumping jack.

(b) Top-view showing extended velocity vectors as the arms and legs move outward.

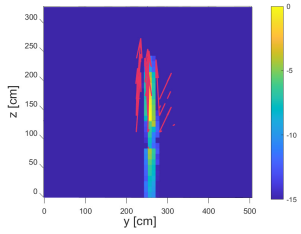

(c) Front-view showing upward velocity vectors as the person leaves the ground.

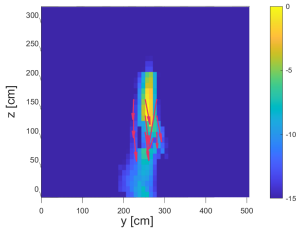

(d) Front-view showing downward velocity vectors as the person returns to the floor.

Fig. 4: Intensity maps and reconstructed velocity vectors (red arrows) of a person performing *jumping jacks* at point X in Fig. 3. (a) and (b) are top-views showing torso and limb motion, with velocity vectors concentrated around the torso (a) and extending outward (b). (c) and (d) are front-views showing vertical motion: upward vectors as the person jumps (c), and downward vectors as the person lands (d).

To further demonstrate the effectiveness of the proposed method for tracking and localizing moving targets, Fig. 5 presents top-view slices of the intensity maps and corresponding velocity vectors for a person walking toward three distinct points: A, B, and C as presented in the sketch of the experimental setup of Fig. 3. The intensity maps illustrate

the person's position while walking, which is in line with the expected location (also empirically cross-checked with the camera recordings); the velocity vectors clearly indicate the direction of motion at the three different spatial locations and time instances.

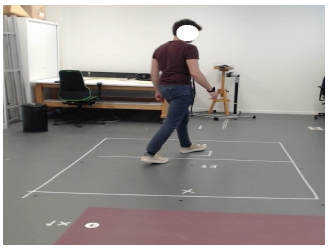

(a) Photograph of the person walking towards point C.

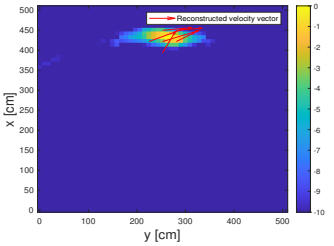

(b) Intensity map & velocity vectors as the person walks toward point C.

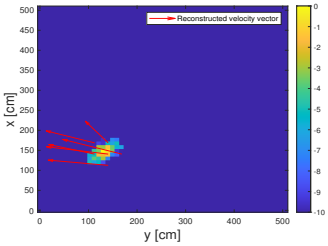

(c) Intensity map & velocity vectors as the person walks toward point B.

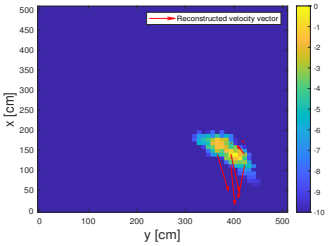

(d) Intensity map & velocity vectors as the person walks toward point A.

Fig. 5: Visualizations of walking motion toward different points. (a) shows a photograph of the subject walking toward point C. (b)–(d) show corresponding intensity maps with velocity vectors for walking toward points C, B, and A, respectively.

As a final example, Fig. 6 compares the three different activities of sitting, turning/restless while lying on the mattress, and kicking/boxing in the air. In Fig. 6b, the top-view of the static, sitting person shows near-zero velocity vectors, reflecting only subtle chest motion due to respiration and small involuntary motions. In contrast, the kicking/boxing activity exhibits the largest velocity vector in the X–Y plane, with $[u_x, u_y] = [-1.55, -0.11]$ m/s, among the three activities, as expected as that movement was performed in a very fast and sudden manner. Regarding the case of turning/restlessness while lying on the mattress, the corresponding intensity map shows a relatively larger footprint of the body on the plane (related to the lying posture seen from a top view), as well as multiple but relatively small velocity vectors, in line with the performed movements.

The presented results demonstrate the feasibility of the proposed method to distinguish dynamic vs static postures with the combination of 3D intensity maps and velocity vectors. This is an important capability for radar-based human monitoring, which can be very useful in the context of private homes, hospital settings, and psychiatric clinics, amongst others.

B. Quantitative Results for Activity Classification

To evaluate the effectiveness of the proposed 3D signatures for HAR, classification is performed using both the intensity maps and reconstructed velocity vectors as input data.

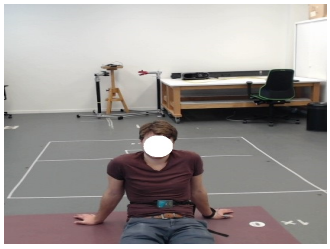

(a) Photograph of the person sitting on the mattress.

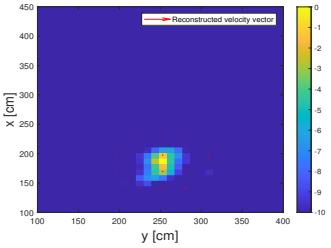

(b) Intensity map & velocity vectors of the person sitting on the mattress.

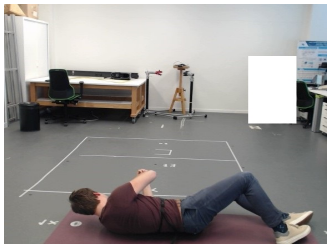

(c) Photograph of the person turning on the mattress while lying.

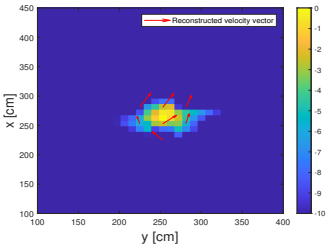

(d) Intensity map & velocity vectors of the person exhibiting turning/restless movement.

(e) Photograph of the person performing boxing/kicking at point X.

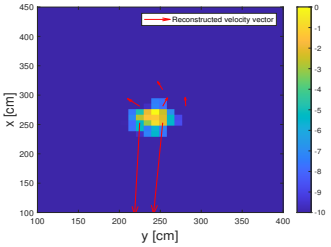

(f) Intensity map & velocity vectors of the person performing boxing/kicking at point X.

Fig. 6: Photographs and corresponding top-view intensity maps with reconstructed velocity vectors (red arrows) of a person performing three different activities: (a)–(b) sitting, (c)–(d) turning/restless while lying on the mattress, and (e)–(f) boxing/kicking in the air.

The reconstructed velocity vector is computed in principle for every voxel in 3D space, but it makes physical sense only when associated with the detected human target [13]. Hence, a spatial mask is applied: voxels within a 50 cm radius around the voxel with the highest intensity value are retained, assuming that this corresponds to the target's location. Furthermore, a percentile-based intensity threshold is used, which keeps only voxels with intensity values above the 95th percentile of the full 3D intensity map, and thus further reduces the noise and focuses on the most significant intensity values.

The measurement area is discretized into a grid of $15 \times 15 \times 15$ cm voxels, aligned with the 15 cm range resolution of the radar setup. The total number of 3D voxels in the grid is $55 \times 55 \times 36$. For each voxel, 3D intensity map $I(x, y, z)$ and voxel-wise velocity vector $\mathbf{U}(x, y, z) = [u_x, u_y, u_z]^T$ are stacked together as input for the neural networks, with each voxel represented by a 4-channel input (intensity plus three

velocity vector components) at each timestamp. Specifically, a 3D CNN is implemented to process this input tensor, comprising three 3D convolutional blocks as depicted in Fig. 7. Each block is composed of a convolutional layer, followed by batch normalization and a ReLU activation function. Max pooling layers are applied after the first and second blocks to reduce the spatial dimensions. For training, a subject-wise 80-20 % holdout is used for the considered dataset of 30 participants, for which basically 24 participants are used for the training set and 6 participants for the testing set. With this, five-fold cross-validation is also performed, whereby the group of 6 participants for the testing set is changed five times in the five folds to include all participants, and the results of the five tests are averaged. A three-class classification

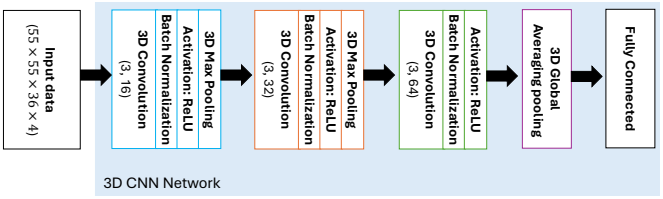

Fig. 7: Structure of the 3D CNN network. Input data is represented as 4-D tensors with intensity values plus 3 components of velocity vectors. The size of convolutional layers is described as [CNN kernel size, number of channels].

task is considered with the following groups of activities: (1) Sitting and Lying on the back, (2) Walking, and (3) Jumping Jacks and Boxing/Kicking. These activities represent contrasting motion characteristics, namely static vs. dynamic activities, and differences between dynamic activities. They are used to assess the ability of the reconstructed 3D signatures in capturing motion strength and directionality, and can be of importance to assess the overall status of patients in a psychiatry context.

For quantitative results, the macro F1 scores for the five folds amount to 98.4 %, 98.7 %, 99.1 %, 96.5 % and 98.5 %, respectively. The averaged macro F1 score over all folds is 98.3 %. Table II depicts the summed confusion matrix across the five folds. It is seen that the results clearly demonstrate the effectiveness of the proposed reconstructed 3D signatures.

TABLE II: Overall Confusion Matrix for 3-Class Classification (i.e., sum of confusion matrices across the testing sets of the five folds)

True / Predicted	Sitting and Laying	Walking	Jumping Jacks, Boxing/Kicking
Sitting and Laying	11977	0	23
Walking	16	5574	213
Jumping Jacks, Boxing/Kicking	30	140	11830

V. Conclusion

This paper demonstrates the use of a 3D reconstruction method for HAR using a network of three distributed 60 GHz MIMO radar nodes. Capon beamforming is applied to generate radar data cubes in range, azimuth, and elevation to build 3D intensity maps, while least-squares optimization is used to reconstruct the voxel-wise velocity vectors from range-Doppler maps. Both static postures and dynamic movements and activities are captured effectively. Consecutive phases of different activities can be recognized by the combination of 3D spatial intensity and related, voxel-wise velocity vectors. Localization of the activity in the area under test is also achieved accurately in the intensity maps. Finally, initial promising results on a three-class classification task are demonstrated (i.e., 98.3% macro F1-score on a five-fold subject-based hold-out validation scheme), by using the reconstructed intensity maps and velocity vector fields as input to a CNN-based classifier.

Acknowledgment

The authors are grateful to all participants for the data collection. This work was partly supported by the Dutch Research Council NWO with their OTP grant *DARE*.

References

[1] C. Li, V. M. Lubecke, O. Boric-Lubecke, and J. Lin, "A review on recent advances in doppler radar sensors for noncontact healthcare monitoring," *IEEE Transactions on microwave theory and techniques*, vol. 61, no. 5, pp. 2046–2060, 2013.

[2] G. Paterniani, D. Sgreccia, A. Davoli, G. Guerzoni, P. Di Viesti, A. C. Valenti, M. Vitolo, G. M. Vitetta, and G. Boriani, "Radar-based monitoring of vital signs: A tutorial overview," *Proceedings of the IEEE*, vol. 111, no. 3, pp. 277–317, 2023.

[3] F. Fioranelli, R. G. Guendel, N. C. Kruse, and A. Yarovoy, "Radar sensing in healthcare: Challenges and achievements in human activity classification & vital signs monitoring," in *International Work-Conference on Bioinformatics and Biomedical Engineering*. Springer, 2023, pp. 492–504.

[4] Y. Kim, I. Alnujaim, and D. Oh, "Human activity classification based on point clouds measured by millimeter wave mimo radar with deep recurrent neural networks," *IEEE Sensors Journal*, vol. 21, no. 12, pp. 13 522–13 529, 2021.

[5] Y. Zhao, A. Yarovoy, and F. Fioranelli, "Angle-insensitive human motion and posture recognition based on 4d imaging radar and deep learning classifiers," *IEEE Sensors Journal*, vol. 22, no. 12, 2022.

[6] F. Fioranelli, M. Ritchie, S. Z. Gürbüz, and H. Griffiths, "Feature diversity for optimized human micro-doppler classification using multistatic radar," *IEEE Transactions on Aerospace and Electronic Systems*, vol. 53, no. 2, pp. 640–654, 2017.

[7] R. Zhang and S. Cao, "Real-time human motion behavior detection via cnn using mmwave radar," *IEEE Sensors Letters*, vol. 3, no. 2, 2018.

[8] S. H. Javadi and A. Farina, "Radar networks: A review of features and challenges," *Information fusion*, vol. 61, pp. 48–55, 2020.

[9] A.-C. Froehlich, D. Mejdani, L. Engel, J. Braeunig, C. Kammel, M. Vossiek, and I. Ullmann, "A millimeter-wave mimo radar network for human activity recognition and fall detection," in *2024 IEEE Radar Conference (RadarConf24)*. IEEE, 2024, pp. 1–5.

[10] S. Waqar, M. Muaaz, and M. Pätzold, "Direction-independent human activity recognition using a distributed mimo radar system and deep learning," *IEEE Sensors Journal*, vol. 23, no. 20, 2023.

[11] S. Scholes, A. Ruget, F. Zhu, and J. Leach, "Human pose inference using an elevated mmwave fmcw radar," *IEEE Access*, vol. 12, 2024.

[12] C. Song, A. D. Droitcour, S. M. M. Islam, A. Whitworth, V. M. Lubecke, and O. Boric-Lubecke, "Unobtrusive occupancy and vital signs sensing for human building interactive systems," *Scientific Reports*, vol. 13, no. 1, p. 954, Jan. 2023.

[13] N. C. Kruse, R. G. Guendel, F. Fioranelli, and A. Yarovoy, "Reconstruction of extended target intensity maps and velocity distribution for human activity classification," *IEEE Transactions on Radar Systems*, vol. 3, 2025.

[14] Texas Instruments, "Iwr6843 and iwr6443 single-chip 60- to 64-ghz mmwave sensor," https://www.ti.com/product/IWR6843.

[15] M. Wendelmuth, A. Yarovoy, and F. Fioranelli, "Breathing rate estimation & apnea detection with multiple elevated and tilted fmcw radars," in *IEEE Radar Conference 2025*, Krakow, Poland, 2025, accepted.